# Influence of Anisotropic Elasticity on Improvement of Liquefaction Predictions: A Multiaxial Approach

*Ali Lashkari*

Assistant Professor, Department of Civil and Environmental Engineering,
Shiraz University of Technology, Shiraz, Iran, e-mail: lashkari@sutech.ac.ir

## ABSTRACT

*It has been revealed that both elastic and plastic components of the granular soils behavior are affected by the stress induced anisotropy as a result of the history of previous shear loadings. While the influence of fabric anisotropy on the plastic elements of the elasto-plastic constitutive models has been extensively studied in the literature, the anisotropic elastic response is usually neglected mainly because of avoiding complication. Herein, a simple anisotropic elasticity theory is proposed. To this aim, the fourth order elasticity tensor is related to a second order fabric-dilatancy tensor describing magnitude and direction of induced anisotropy. Proper constitutive equations for calibration of the proposed elasticity theory using data of triaxial and simple shear tests are presented. Then, the introduced elasticity theory is implemented within an advanced sand constitutive model. The model predictions are compared with the experimental data of independent research teams. It is shown that the modification of the basic platform by the proposed anisotropic elasticity theory leads to improvement of liquefaction predictions.*

## 1. Introduction

Occurred on June 20, 1990 in northern areas of Iran, the disastrous Manjil Earthquake ($M$ = 7.3) is still considered among the strongest registered seismological events of the region. After the earthquake, the signs of earthquake induced liquefaction were extensively observed in the fluvial plain of the Sefidrood River. In two particular areas in Astaneh city ($a_{max}/g \approx$ 0.15-0.20), severe damage to wooden framed brick residential houses due to liquefaction has been reported. In these areas, very loose sand layers ($N_{SPT}$ = 3-10 at depth of about 7$m$) were found, which were very prone to liquefaction under seismic loads. In Roodbaneh, a small local town about 7$km$ east of Astaneh, the main road through the town and the roadside houses were suffered from the liquefaction induced lateral spreading (horizontal movement about 200$cm$ together with 50$cm$ settlement). Besides, the liquefaction in Roodbaneh induced

a small-scale slide as a result of the low value of the mobilized shear stress in the liquefied stratum. A detailed investigation of the geotechnical aspects of the Manjil Earthquake can be found in Ishihara et al [1]. Loose saturated granular soils are very common in costal urban and industrial areas in both north and south of Iran. In addition, from a seismological view, both regions are very active. Hence, the possibility of injuries due to liquefaction induced phenomena indicates further studies on the mechanisms of liquefaction and their remedy.

Understanding the mechanical behavior of granular soils subjected to shear stress and the related constitutive modeling are of great interest in soil mechanics and geotechnical engineering. As a consequence, this issue has been the subject of many sophisticated studies in the past decades, e.g. [2-19]. Been and Jefferies [2] suggested that the current

state of granular soils can be measured by two state variables: (a) a state parameter which takes into account the combined influence of density and mean principal effective stress, and (b) a fabric state parameter which quantifies the micro-scale characteristics of granular media based on the geometrical factors such as the orientation of voids, normal vectors to the contact planes between grains, and the preferred orientation of grains. A glance at the literature indicates that this suggestion has been the cornerstone of many innovations in the field of constitutive modeling in the recent decades. Using the state diagram, Been and Jafferies [2] introduced a state parameter based on the distance of the current soil state from a conjugate state on the critical state line with the same value of mean principal effective stress. Since then, it has been shown that the proposed state parameter of Been and Jefferies [2] may not be unique and other effective state parameters have been introduced, e.g. [12, 16, 20, 21, 22]. Following the suggestion of Muir Wood et al [23], a number of state-dependent constitutive models were created, e.g. [11, 12, 21, 24]). By incorporating state parameters in their formulation, these constitutive models are capable of providing reasonable predictions for the mechanical behavior of sands over wide ranges of states by using a unique set of parameters. The other major advancement has been achieved in the last decade by considering the influence of fabric anisotropy in sands constitutive modeling, e.g. [14, 18, 19, 25, 26]. In these models, some ingredients of the previous generation of constitutive models were related to fabric tensors to improve their predictive capacity to consider various aspects of the anisotropic behavior of granular soils. The fundamental studies using photo-elastic materials and Discrete Element Method have indicated that the history of previous shear loadings (specially the last one) may leave remarkable anisotropy in granular media, e.g. [27-31]. The anisotropy leads to the strong tendency of granular soils to contract (say to pore pressure build up) in unloading parts of the butterfly loop in constant volume stress paths. The butterfly loop is generally where the sand state steps in liquefaction and post-liquefaction state. Hence, any success in constitutive modeling of sands in the butterfly loop conveys a victory in liquefaction modeling. By using a fabric-dilatancy tensor, Papadimitriou et al [25] introduced a modified plastic hardening modulus to simulate this particular

behavior. Dafalias and Manzari [18] suggested a modified dilatancy function that leads to a massive contraction in unloading portions of the butterfly loop. In all theoretical works described above [9-19] and [21-25], it has been assumed that the elastic part of the behavior remains isotropic even at very large shear deformation when the fabric of soil becomes highly anisotropic. This assumption is not realistic, and experimental studies have shown that the elastic part of behavior also becomes anisotropic when geomaterials are subjected to large shear deformations, e.g., [5, 32-34].

In this study, based on the physical consideration on sand response subjected to undrained shearing, a simplified anisotropic elasticity theory is proposed in section 3. Detailed formulation of the bounding surface plasticity model of Dafalias and Manzari [18] in multiaxial stress and strain spaces is presented in section 4. Then, the introduced elasticity is implemented within the bounding surface plasticity platform. Finally, the modified model is evaluated against monotonic and cyclic data in section 5.

## 2. Re-Visiting the Isotropic Elasticity Theory and its Limitations in Modeling of Granular Soils

Assuming a linear dependence between the rates of stress and the corresponding strain tensors, the most fundamental constitutive equation in elasticity theory is:

$$\dot{\boldsymbol{\sigma}} = \boldsymbol{E}\dot{\boldsymbol{\varepsilon}}^e \tag{1}$$

where $\boldsymbol{\sigma}$ and $\boldsymbol{\varepsilon}$ are respectively the second rank stress and strain tensors. $\boldsymbol{E}$, the elasticity tensor, is a forth rank tensor whose main role is defining pro-portionality in Eq. (1). Using the representation theorem for isotropic functions, it has been shown that the most general form of $\boldsymbol{E}$ for isotropic materials can be represented by [e.g. 35]:

$$E_{ijkl} = \phi_1 \, \delta_{ij}\delta_{kl} + \phi_2(\delta_{ik}\delta_{jl} + \delta_{il}\delta_{jk}) \tag{2}$$

where $\phi_i$ ($i = 1, 2$) are material constants. Eq. (2) indicates that the minimum number of independent material parameters for constitutive modeling of the elastic behavior of isotropic continuums is two. Recalling the conventional forms of isotropic elasticity in continuum mechanics, one can conclude that $\phi_i$ ($i = 1, 2$) should be functions of Lame constants. For example, replacing $\phi_1$ and $\phi_2$, respectively, by ($K$-2/3$G$) and $G$, Eq. (2) is transformed into the following familiar form:

$$E_{ijkl} = (K - 2/3\,G)\,\delta_{ij}\delta_{kl} + G(\delta_{ik}\delta_{jl} + \delta_{il}\delta_{jk}) \qquad (3)$$

where, $G$ and $K$ are, respectively, the elastic shear and bulk moduli which may be measured using very small strain (shear strain less than $10^{-6}$ in soils) testing techniques such as resonant column or bender element.

As a result of the incomparable simplicity in both realization and application, the theory of isotropic elasticity (Eqs. (1) to (3)) has been widely employed in engineering sciences, including geomechanical engineering. The backbone of the isotropic elasticity theory is based on the experiments on metals, especially steel; however, a substantial difference exists between the nature of metals and geomaterials (e.g., soils). In the recent years, the micromechanical response of granular media has been extensively studied in laboratory using photoelastic materials in conjunction with image analysis, and by numerical methods such as Discrete Element Method [e.g., 27-31]. These studies have revealed that when granular soils are subjected to shear stress, they gain their strength by creating new force chains as well as strengthening the existing ones oriented toward the major principal stress axes. These phenomena are accompanied by weakening or erasing those weak force chains in the opposite direction (toward the minor principal stress direction). It is worth noting that the applied external loads are transferred in granular media through the network of the mentioned force chains. Having the same trend, it has been reported that grains in sheared granular media re-arrange their contact points in such a way that the normal vectors to their contact points tend to be oriented towards the major principal stress direction [e.g., 27-31]. Rose diagrams drawn based on the direction of normal vectors to the contact points between grains indicate that the fabric of initially isotropic granular materials becomes gradually anisotropic by applying shear stress. The fabric evolution is accelerated when the volume change response becomes dilative (after the initial transient contraction). Finally, the fabric anisotropy reaches a saturate state at large shear strains.

The observed behavior of granular materials from the micromechanical perspective shows that the fabric of such media becomes anisotropic when they are subjected to shear stress. As a consequence, the reliability of the assumption of the isotropic elastic behavior of granular soils should be re-

evaluated. Surprisingly, experimental works do not support the assumption of isotropic elasticity for granular soils under shear [e.g., 5, 32, 33, 34]. To investigate this issue, the result of an undrained simple shear test in torsional shear apparatus [5] is presented in Figure (1). In this test, a number of small unloading-reloading cycles were imposed on the sample during the main loading, see Figure (1a).
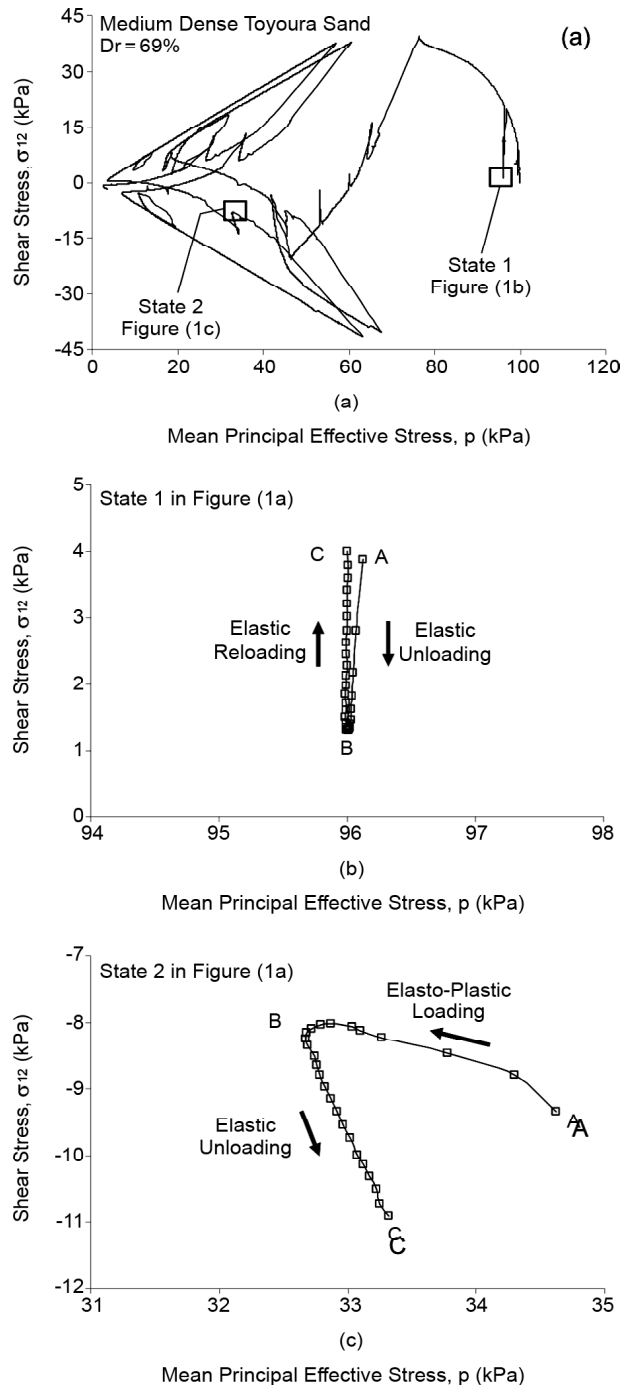


**Figure 1.** Effective stress path a cyclic torsion shear test: (a) the complete stress paths; (b) an elastic unloading-reloading cycle in contractive part of behavior; (c) an elastoplastic loading-elastic unloading cycle in dilative part of behavior (data from [5]).

The measured behaviors of the sample in two different states "1" and "2" are considered in parts "b" and "c" of Figure (1). The sample was in contractive phase and mean principal effective stress decreased gradually before the sample was subjected to a small elastic unloading-reloading cycle in state "1", see parts "a" and "b" of Figure (1). It is observed that the slope of the tangents to *AB* and *BC* with respect to the p-axis is nearly vertical. The sample has experienced a massive dilation in elastoplastic loading path, see *AB* in Figure 1(c), which followed by an elastic unloading, see *BC* in Figure (1c) in state "2". It is widely accepted that the unloading behavior of soils immediately after elastoplastic loading is rather pure elastic. Hence, the path *BC* in Figure (1c) is also representative of the elastic response of the soil sample. Comparing the paths *BC* in parts "b" and "c", one can find that in part "c" the slope of the tangent to the elastic path with respect to the p-axis is not vertical (the same scale is used for the vertical and horizontal axes of both figures). Now, we re-visit Eq. (3) in conjunction with Eq. (1) to discover whether the isotropic theory is capable of simulating these behaviors or not. For simple shear loading, the isotropic elastic response results in:

$$\dot{\sigma}_{12} = 2G\,\dot{\varepsilon}_{12}^{e} \tag{4}$$

$$\dot{p} = (\dot{\sigma}_{11} + \dot{\sigma}_{22} + \dot{\sigma}_{33})/3 = K\,\dot{\varepsilon}_{v}^{e} = 0 \tag{5}$$

To clarify the outcome of Eq. (5), it must be noted that drainage is not allowed, and therefore, the volumetric strain rate becomes zero in undrained shear. As a consequence, the rate of mean principal effective stress, $\dot{p}$, should be zero under undrained simple shear loading when the material behavior is assumed both isotropic and elastic. At each stress state on stress path, the ratio $\dot{\sigma}_{12}/\dot{p}$ indicates the instantaneous slope of the tangent to the stress path. Considering Eqs. (4) and (5), value of the ratio $\dot{\sigma}_{12}/\dot{p}$ is always infinite for isotropic elastic materials subjected to undrained simple shear, and the stress paths of such materials should be vertical with respect to the p-axis. By referring to Figure (1b), it is observed that the slope of the tangent to the elastic unloading and elastic re-loading stress paths are nearly vertical. This means that the initial and induced anisotropy at state "1" are negligible. In an opposite manner, a remarkable deviation from the vertical

direction can be observed for the tangent to the elastic unloading path (*BC*) in Figure (2c) that corroborates the existence of a remarkable anisotropy at state "2". Based on the presented experiment result, the following points can be concluded: (1) the assumption of isotropic elasticity is not reasonable in granular soils; and (2) anisotropy evolves mainly in the dilative portion of behavior. These points are the cornerstone of the modification proposed in this study.

## 3. Effect of Induced Anisotropy on Elastic Response

Although the anisotropic elasticity theory has not yet been well considered in geomechanical engineering applications, a large number of revolutionary studies on this issue have been published in the literature by the mathematicians and the researchers who work on the theoretical fields of the mechanical engineering. There are numerous methods suggested by researchers accounting for the influence of anisotropy on the elastic response of materials. For example, by using the representation theorem for isotropic functions, it has been shown that the most general form of $E_{ijkl}$ for anisotropic materials is [e.g., 36-38]:

$$
\begin{aligned}
E_{ijkl} = {} & \phi_1\,\delta_{ij}\delta_{kl} + \phi_2(\delta_{ik}\delta_{jl} + \delta_{il}\delta_{jk}) \\
& + \phi_3(Z_{ij}\delta_{kl} + Z_{kl}\delta_{ij}) \\
& + \phi_4(Z_{ik}\delta_{jl} + Z_{il}\delta_{jk} + Z_{jk}\delta_{il} + Z_{jl}\delta_{ik}) \\
& + \phi_5 Z_{ij}Z_{kl} + \phi_6(Z_{ik}Z_{jl} + Z_{il}Z_{jk}) \\
& + \phi_7(Z_{im}Z_{mj}\delta_{kl} + Z_{km}Z_{ml}\delta_{ij}) \\
& + \phi_8(Z_{im}Z_{mk}\delta_{jl} + Z_{im}Z_{ml}\delta_{jk} \\
& \quad + Z_{jm}Z_{mk}\delta_{il} + Z_{jm}Z_{ml}\delta_{ik}) \\
& + \phi_9(Z_{im}Z_{mj}Z_{kl} + Z_{ij}Z_{km}Z_{ml}) \\
& + \phi_{10}(Z_{im}Z_{mk}Z_{jl} + Z_{ik}Z_{jm}Z_{ml} \\
& \quad + Z_{im}Z_{ml}Z_{jk} + Z_{im}Z_{ml}Z_{jk}) \\
& + \phi_{11}(Z_{im}Z_{mj}Z_{kn}Z_{nl}) \\
& + \phi_{12}(Z_{im}Z_{mk}Z_{jn}Z_{nl} + Z_{im}Z_{ml}Z_{jn}Z_{nk})
\end{aligned} \tag{6}
$$

where, $\phi_i$ ($i = 1$-12) are independent material parameters which are functions of $tr\mathbf{Z}$, $tr\mathbf{Z}^2$, and $tr\mathbf{Z}^3$; and $\mathbf{Z}$ is a proper traceless fabric tensor. The concept of fabric tensor has been introduced to characterize the spatial distribution of micromechanical geometric properties of geomaterials such as direction of contact planes between grains and their evolution with shear stress [35, 39, 40, 41]. The most

general form of a second order fabric tensor, $H_{ij}$, is [35]:

$$H_{ij} = \frac{1}{4\pi} \int_{\Omega} H(\Omega) \varpi_i \varpi_j d\Omega \qquad (7)$$

where, the function $H(\Omega)$ denotes the spatial statistical distribution of an anisotropic micromechanical property such as the distribution of normal vectors to the contact planes. $\Omega$ represents the surface of a unit sphere used for calculation of Eq. (7). For the selected configuration, $\varpi_r \, (r = 1\text{-}3)$ are the direction cosines of normal vector to the contact planes. Based on Eq. (7), the most general traceless fabric tensor, $Z$, becomes:

$$Z = H - 1/3(trH) \, I \qquad (8)$$

For isotropic materials, $Z = 0$ and Eq. (6) transforms into Eq. (2).

According to Eq. (6), at least twelve independent material parameters are required if one attempts to consider the influence of fabric anisotropy in a complete manner. The importance of this issue becomes much apparent when it is noted that the whole number of parameters in the recent well-known constitutive models such as MIT-S1 [13], UBCSAND [17], and in SANISAND [11, 18, 25] is 13, 9, and 15, respectively. Thus, the application of the anisotropic elasticity theory of Eq. (6) in its complete form nearly doubles the number of the model parameters which is undesirable. To overcome this limitation, it is decided to use a truncated form of $E_{ijkl}$, which only takes into account the influence of terms with the first order of dependence on $Z$:

$$
\begin{aligned}
E_{ijkl} = & \; \phi_1 \, \delta_{ij}\delta_{kl} + \phi_2 (\delta_{ik}\delta_{jl} + \delta_{il}\delta_{jk}) \\
& + \phi_3 (Z_{ij}\delta_{kl} + Z_{kl}\delta_{ij}) \\
& + \phi_4 (Z_{ik}\delta_{jl} + Z_{il}\delta_{jk} + Z_{jk}\delta_{il} + Z_{jl}\delta_{ik})
\end{aligned} \qquad (9)
$$

In the following lines, it is shown that the above selection is capable of describing the instantaneous slope of the tangents to the stress paths at any given points on very small unloading-reloading cycles.

### 3.1. Selection of Proper Parameters for the Aniso-tropic Elasticity Tensor

By using Eq. (1) in conjunction with Eq. (9), trace of the stress rate tensor becomes:

$$
\begin{aligned}
\dot{\sigma}_{mm} = E_{mmkl}\, \dot{\varepsilon}_{kl}^e = & \{ \phi_1 \, \delta_{mm}\delta_{kl} \\
& + \phi_2 (\delta_{mk}\delta_{ml} + \delta_{ml}\delta_{mk}) \\
& + \phi_3 (Z_{mm}\delta_{kl} + Z_{kl}\delta_{mm}) \\
& \phi_4 (Z_{mk}\delta_{ml} + Z_{ml}\delta_{mk} + Z_{mk}\delta_{ml} + Z_{ml}\delta_{mk}) \} \dot{\varepsilon}_{kl}^e
\end{aligned} \qquad (10)
$$

Considering that $Z$ is a traceless tensor (i.e., $trZ = 0$) and $\dot{p} = (1/3)\dot{\sigma}_{mm}$, ordinary algebra operations reduce Eq. (10) to:

$$\dot{p} = \frac{1}{3}\dot{\sigma}_{mm} = (\phi_1 + \frac{2}{3}\phi_2)\dot{\varepsilon}_{kk}^e + (\phi_3 + \frac{4}{3}\phi_4) Z_{kl}\, \dot{e}_{kl}^e \qquad (11)$$

The rate of shear stress tensor is calculated by:

$$
\begin{aligned}
\dot{s}_{ij} = & \; \dot{\sigma}_{ij} - (1/3)\dot{\sigma}_{mm}\delta_{ij} \\
= & \; \phi_1 \{ \delta_{ij}\delta_{kl}\dot{\varepsilon}_{kl}^e - \dot{\varepsilon}_{kk}^e\delta_{ij} \} + \\
& \phi_2 \{ (\delta_{ik}\delta_{jl} + \delta_{il}\delta_{jk})\dot{\varepsilon}_{kl}^e - \frac{2}{3}\dot{\varepsilon}_{kk}^e\delta_{ij} \} + \\
& \phi_3 \{ (Z_{ij}\delta_{kl}\dot{\varepsilon}_{kl}^e + Z_{kl}\delta_{ij}\dot{\varepsilon}_{kl}^e) - Z_{kl}\dot{e}_{kl}^e\delta_{ij} \} + \\
& \phi_4 \{ (Z_{ik}\delta_{jl} + Z_{il}\delta_{jk} + Z_{jk}\delta_{il} + Z_{jl}\delta_{ik})\dot{\varepsilon}_{kl}^e - \frac{4}{3}Z_{kl}\dot{e}_{kl}^e\delta_{ij} \}
\end{aligned} \qquad (12)
$$

Some ordinary algebra leads to the following expression for the rate of shear stress tensor:

$$
\begin{aligned}
\dot{s}_{ij} = & \; 2\phi_2 \dot{e}_{ij}^e + \phi_3 \, Z_{ij}\dot{\varepsilon}_{kk}^e + \\
& \phi_4 \{ 2(Z_{ik}\dot{e}_{kj}^e + Z_{kj}\dot{e}_{ki}^e) + \frac{4}{3}Z_{ij}\dot{\varepsilon}_{mm}^e - \frac{4}{3}Z_{kl}\dot{e}_{kl}^e\delta_{ij} \}
\end{aligned} \qquad (13)
$$

Hence, the ratio $\dot{s}_{ij} / \dot{p}$ can be calculated by:

$$
\begin{aligned}
\frac{\dot{s}_{ij}}{\dot{p}} = & \; \frac{2\phi_2 \dot{e}_{ij}^e + \phi_3 \, Z_{ij}\dot{\varepsilon}_{kk}^e}{(\phi_1 + \frac{2}{3}\phi_2)\dot{\varepsilon}_{kk}^e + (\phi_3 + \frac{4}{3}\phi_4) Z_{kl}\dot{e}_{kl}^e} + \\[2mm]
& \frac{\phi_4 \{ 2(Z_{ik}\dot{e}_{kj}^e + Z_{kj}\dot{e}_{ki}^e) + \frac{4}{3}Z_{ij}\dot{\varepsilon}_{mm}^e - \frac{4}{3}Z_{kl}\dot{e}_{kl}^e\delta_{ij} \}}{(\phi_1 + \frac{2}{3}\phi_2)\dot{\varepsilon}_{kk}^e + (\phi_3 + \frac{4}{3}\phi_4) Z_{kl}\dot{e}_{kl}^e}
\end{aligned} \qquad (14)
$$

As mentioned before, slope of the tangent to stress path can be used as a description of fabric anisotropy. In this regard, slope of the tangent to stress path is determined by the ratio $\dot{q}/\dot{p} \, (= \dot{s}_{11}/\dot{p} - \dot{s}_{33}/\dot{p})$ in constant volume triaxial loading. For the case of simple shear, the ratio $\dot{s}_{12}/\dot{p}$ can be used to describe the slope of the tangent to stress path. The same trend can be found for unconventional stress paths. It is observed that in all cases, having the ratio $\dot{s}_{ij}/\dot{p}$ is an essential factor.

In a general undrained (constant volume) shear test, Eq. (14) is reduced to:

$$\frac{\dot{s}_{ij}}{\dot{p}} = \frac{2\phi_2\,\dot{e}_{ij}^e + \phi_4\left\{2(Z_{ik}\dot{e}_{kj}^e + Z_{kj}\dot{e}_{ki}^e) - \frac{4}{3}Z_{kl}\dot{e}_{kl}^e\delta_{ij}\right\}}{(\phi_3 + \frac{4}{3}\phi_4)\,Z_{kl}\,\dot{e}_{kl}^e} \quad (15)$$

An example of such a test described above is schematically shown in Figure (2). It was started at isotropic stress state ($p = 284kPa$). Then it was subjected to undrained shear with the maximum amplitude $= 150kPa$. During the reversal points $R1$ and $R2$, the sample stress path formed a butterfly loop which is a signal of cyclic mobility. In $R1$ and $R2$, the fabric is nearly in fully anisotropic saturate state, which indicates that if the current loading is followed to the critical state, the excessive shearing would not result in further evolution of fabric. Fabric is a direction-dependent property. Hence, due to the opposite directions of loading prior to $R1$ and $R2$, signs of the corresponding terms in fabric tensor for $R1$ and $R2$ should be opposite; however, their magnitudes are nearly the same. Immediately after $R1$ and $R2$, the sample is elastically unloaded. The tangents to the stress path at $R1$ and $R2$ are illustrated in Figure (2). It is observed that the slopes of the tangent lines are opposite, but the values of the slopes with respect to the p-axis are relatively the same, because at both points fabric is nearly in saturate state. Considering this discussion, the terms $(\phi_3 + 4/3\phi_4)Z_{kl}\,\dot{e}_{kl}^e$ and $\phi_4[2(Z_{ik}\dot{e}_{kj}^e + Z_{kj}\dot{e}_{ki}^e) - (4/3)Z_{kl}\dot{e}_{kl}^e\delta_{ij}]$ does not change sign upon reversal (because at loading reversal points, signs of $Z$ and $\dot{e}^e$ are always the same); however, the sign of the term $2\phi_2\,\dot{e}_{ij}^e$ changes with the change of shear strain direction. Moreover, it was also discussed that the slopes of the tangent lines at $R1$ and $R2$ have the same values but the opposite signs. Considering these points, the latter phenomenon is not possible unless $\phi_4$ becomes zero. Referring to Eqs. (2) and
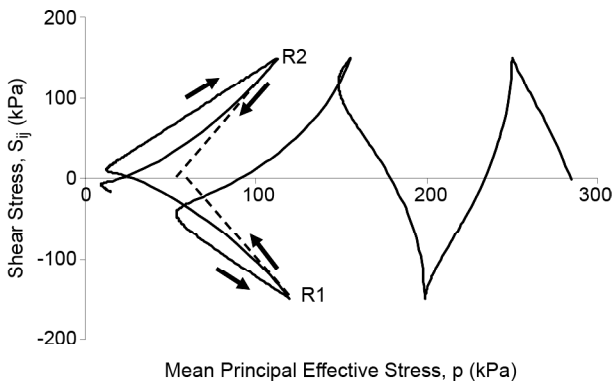


**Figure 2.** A typical constant volume test in $s_{ij}$-p plane.

(3) for isotropic condition ($Z=0$), $\phi_1 = K - 2/3G$, and $\phi_3 = G$ are selected. Moreover, by changing notation $\Phi = \phi_3$, the following constitutive equations are obtained:

$$\dot{p} = \frac{1}{3}\dot{\sigma}_{mm} = K\dot{\varepsilon}_{kk}^e + \Phi\,Z_{kl}\,\dot{e}_{kl}^e = K\dot{\varepsilon}_v^e + \Phi\,\mathbf{Z}:\dot{\mathbf{e}}^e \quad (16)$$

$$\dot{s}_{ij} = 2G\dot{e}_{ij}^e + \Phi\,Z_{ij}\,\dot{\varepsilon}_{kk}^e = 2G\dot{\mathbf{e}}^e + \Phi\,\mathbf{Z}\dot{\varepsilon}_v^e \quad (17)$$

$$\frac{\dot{s}_{ij}}{\dot{p}} = \frac{2G\dot{e}_{ij}^e + \Phi\,Z_{ij}\,\dot{\varepsilon}_{kk}^e}{K\dot{\varepsilon}_{kk}^e + \Phi\,Z_{kl}\,\dot{e}_{kl}^e} = \frac{2G\dot{\mathbf{e}}^e + \Phi\,\mathbf{Z}\dot{\varepsilon}_v^e}{K\dot{\varepsilon}_v^e + \Phi\,\mathbf{Z}:\dot{\mathbf{e}}^e} \quad (18)$$

By considering Eq. (16), it is observed that the presence of fabric anisotropy ($\mathbf{Z} \neq 0$) results in the dependence of the rate of mean principal stress on both elastic volumetric and shear strains. A similar coupling for the shear stress tensor can be found in Eq. (17). For the case of isotropy ($\mathbf{Z} = 0$), Eqs. (16) to (18) are reduced to the conventional elasticity.

### 3.2. Calculation of $\Phi$ Using Conventional Tests

An agreed versatile fabric tensor fitting all aspects of the mechanical behavior of granular media is not available at this time; however, there are some suggestions in the literature which can be applied for particular purposes. Herein, the fabric-dilatancy tensor of Dafalias and Manzari [18] with the following evolution law is adopted:

$$\dot{\mathbf{Z}} = c_z\langle -\dot{\varepsilon}_v^p\rangle[Z_{max}\,\mathbf{n} - \mathbf{Z}] \quad (19)$$

where, $c_z$ and $Z_{max}$ are material constants. This evolution law fulfills many of the previously described requirements, including: (1) direction dependency; (2) evolution with dilation; and (3) the existence of a saturate state.

In practice, $G$ and $K$, see Eqs. (16) and (17), can be measured using resonant column, bender element, or any other small amplitude shear tests. As previously discussed, valuable data on the evolution of anisotropy may be extracted from the slope of the tangents to constant volume stress paths. When the soil state enters the dilative part of the butterfly loop, the fabric (and hence, the fabric tensor) is in saturate or nearly saturate state. By using these points and Eq. (19), one can obtain the following relationship for the slope of the tangent to stress path in constant volume triaxial tests immediately after unloading in a butterfly loop:

$$\left|\beta_{TX}\right| = \left|\frac{\dot{q}}{\dot{p}}\right| = \frac{\sqrt{6}\,G}{\varPhi\,Z_{max}} \qquad (20)$$

where, $\beta_{TX}$ is slope of the tangent to stress path in the butterfly loop immediately after unloading, and $q$ (deviator stress) $= \sigma_1 - \sigma_3$. By rearrangement of terms, one has:

$$\varPhi = \frac{\sqrt{6}\,G}{Z_{max}\left|\beta_{TX}\right|} \qquad (21)$$

Study of available liquefaction data indicates that $\left|\beta_{TX}\right| \approx 3$ is a good estimation for various sands. This can simplify Eq. (21) to the following form:

$$\varPhi \approx \frac{0.8\,G}{Z_{max}} \qquad (22)$$

Finally, performing the same calculations for simple (torsional) shear tests leads to:

$$\varPhi = \frac{\sqrt{2}\,G}{Z_{max}\left|\beta_{SS}\right|} \qquad (23)$$

where, $\beta_{SS}$ is the slope of the tangent to stress path in undrained simple (torsional) shear tests (measured in $\sigma_{12}$-$p$ plane). In the proposed anisotropic elasticity theory, $\varPhi$ plays the role of the third elastic moduli which can be calibrated by Eqs. (21) to (23).

## 4. General Formulation of a Bounding Surface Sand Plasticity Model

For implementation of the proposed anisotropic elasticity, the critical state compatible bounding surface plasticity model of Dafalias and Manzari [18] is selected. In the following lines, detailed formulation of this model is described.

Total strain rate tensor is decomposed into the elastic and plastic parts:

$$\dot{\boldsymbol{\varepsilon}} = \dot{\boldsymbol{\varepsilon}}^{e} + \dot{\boldsymbol{\varepsilon}}^{p} \qquad (24)$$

where superscripts "e" and "p" indicate the elastic and plastic branches. The elastic part of strain rate tensor is calculated here by the anisotropic elasticity theory presented in the last section. In the absence of low amplitude shear tests, $G$ and $K$ can be estimated by experimental correlations suggested by Hardin and Richart [42]:

$$G = G_0\,p_{ref}\,\frac{(2.97 - e)^2}{(1 + e)}\sqrt{\frac{p}{p_{ref}}} \qquad (25)$$

$$K = \frac{2}{3}\,G\left(\frac{1 + \nu}{1 - 2\nu}\right) \qquad (26)$$

in Eq. (25), e is the current value of void ratio, and $p_{ref}$ is a reference pressure that can be taken as the atmospheric pressure ($\approx 101\,kPa$). In its definition, the elastic bulk modulus in Eq. (26) is related to the elastic shear modulus through the Poisson's ratio ($\nu$). Regarding the third elastic modulus, $\varPhi$ is calculated using Eqs. (21)-(23).

Yield surface describes domain of pure elasticity in multiaxial stress space:

$$f(\boldsymbol{\sigma}, \boldsymbol{\alpha}) = [(\boldsymbol{s} - p\boldsymbol{\alpha}) : (\boldsymbol{s} - p\boldsymbol{\alpha})]^{1/2} - \sqrt{2/3}\,mp = 0 \quad (27)$$

Yield surface of Eq. (27) has a cone shape with circular cross section in principal stress space and its apex is fixed on the origin of stress space. $\boldsymbol{\alpha}$ is back-stress ratio which is a second order traceless tensor indicating the location of the yield surface axis in deviator plane, see Figure (3). Plastic strains may be generated when stress state reaches the yield surface and attempts to move beyond its domain. At such a moment, the gradient to the yield
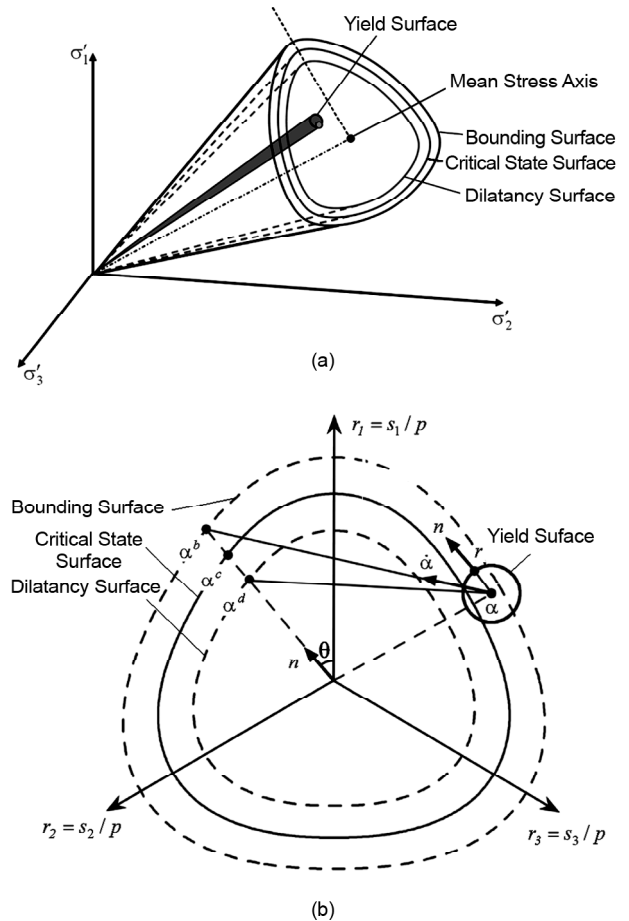


**Figure 3.** Schematic view of the model constitutive surfaces.

surface becomes:

$$L = \frac{\partial f(\boldsymbol{\sigma}, \boldsymbol{\alpha})}{\partial \boldsymbol{\sigma}} = \boldsymbol{n} - (1/3) N \boldsymbol{I} \tag{28}$$

where,

$$\boldsymbol{n} = \frac{\boldsymbol{r} - \boldsymbol{\alpha}}{\sqrt{2/3}\, m} \quad ; \quad N = \boldsymbol{n} : \boldsymbol{r} \tag{29}$$

In above equations, $\boldsymbol{r}(= \boldsymbol{s}/p)$ is shear stress ratio tensor, and $\boldsymbol{n}$ is a traceless unit tensor ($\boldsymbol{n} : \boldsymbol{n} = 1$) indicating the yield direction in deviator ($\pi$) plane, see Figure (3).

By adopting a non-associated flow rule, the plastic strain rate is calculated by:

$$\dot{\boldsymbol{\varepsilon}}^p = \langle \Lambda \rangle \, \boldsymbol{R} = \langle \Lambda \rangle [\boldsymbol{n} + (1/3) D \boldsymbol{I}] \tag{30}$$

where $D$ is dilatancy function, and $\Lambda$ is loading index which indicates the magnitude of plastic shear strain rate. These terms are introduced in followings.

In addition to the yield surface, the model employs three other constitutive surfaces: the bounding, the critical, and the dilatancy surfaces, see Figure (3). Bounding surface defines domain of accessible stresses. Critical state surface is the locus of stress states of the samples reached critical state. Finally, dilatancy surface describes a reference boundary separating contractive states from those states in which the behavior is dilative. The model constitutive surfaces in multiaxial stress space are mathematically expressed by:

$$\boldsymbol{\alpha}^b(\theta) = \sqrt{2/3}\,[g(\theta, c) M_b - m] \boldsymbol{n} \tag{31}$$

$$\boldsymbol{\alpha}^c(\theta) = \sqrt{2/3}\,[g(\theta, c) M_b - m] \boldsymbol{n} \tag{32}$$

$$\boldsymbol{\alpha}^d(\theta) = \sqrt{2/3}\,[g(\theta, c) M_b - m] \boldsymbol{n} \tag{33}$$

where $\boldsymbol{\alpha}^b(\theta), \boldsymbol{\alpha}^c(\theta)$, and $\boldsymbol{\alpha}^d(\theta)$ are, respectively, back stress ratios corresponding to the bounding, the critical, and the dilatancy surfaces. $g(\theta, c)$ is a proper interpolation function which takes into account the actual shape of bounding, critical, and dilatancy surfaces in deviator $\pi$-plane. $\theta$ is the Lode angle, and $c$ is defined by the ratio $M_e/M_c$. In this definition, $M_c$ and $M_e$ are respectively the slopes of critical state line measured in the compression and extension modes of triaxial. $M_b$ and $M_d$ are the sizes of the bounding and dilatancy surfaces measured in triaxial compression:

$$M_b = M_c \exp(-n_b \psi) \tag{34}$$

$$M_d = M_c \exp(n_d \psi) \tag{35}$$

where, $n_b$ and $n_d$ are two model parameters, and $\Psi$ is the state parameter [2]:

$$\psi = e - e_c = e - [e_\Gamma - \lambda(p/p_{ref})^\xi] \tag{36}$$

In Eq. (36), $e_c$ is the critical void ratio corresponding to the current value of mean principal effective stress. $e_\Gamma$ and $\lambda$ are the model parameters.

Dilatancy function is defined by, see Eq. (30):

$$D = A(1 + \langle - \boldsymbol{Z} : \boldsymbol{n} \rangle) \, \boldsymbol{d} : \boldsymbol{n} \tag{37}$$

where, $\boldsymbol{d} = \boldsymbol{\alpha}^d(\theta) - \boldsymbol{\alpha}$ is distance between the current back-stress ratio and a conjugate back-stress ratio on the dilatancy surface, and $A$ is a model parameter. The presence of fabric tensor in definition of dilatancy enables the constitutive model to take into account the influence of induced anisotropy on the plastic portion of behavior.

To consider the possibility of kinematic hardening of the yield surface, plastic hardening modulus is defined by:

$$K_p = H(e) G \frac{\boldsymbol{b} : \boldsymbol{n}}{(\boldsymbol{\alpha} - \boldsymbol{\alpha}_{in}) : \boldsymbol{n}} \tag{38}$$

where, $H(e)$ is a parameter which depends on void ratio. $\boldsymbol{b} = \boldsymbol{\alpha}^b(\theta) - \boldsymbol{\alpha}$ is distance between the current back-stress ratio and a conjugate back-stress ratio on the bounding surface. The geometrical rule to find conjugate points on the bounding and dilatancy surfaces is illustrated in Figure (3b).

### 4.1. Explicit form of the Constitutive Equations

Loading index, $\Lambda$, see Eq. (30) is calculated by:

$$\Lambda = \frac{1}{K_p} \cdot \frac{\partial f}{\partial \boldsymbol{\sigma}} : \dot{\boldsymbol{\sigma}} \tag{39}$$

It is preferred to calculate the loading index based on total stain rates, soil moduli, dilatancy function and fabric tensor. This goal can be achieved by considering Eqs. (16), (17), (28), (29) and (30) into Eq. (39) and performing some algebra operations which yield to:

$$\Lambda = \frac{(2G\boldsymbol{n} - \Phi N \boldsymbol{Z}) : \dot{\boldsymbol{e}} + (\Phi \boldsymbol{n} : \boldsymbol{Z} - NK)\dot{\varepsilon}_v}{K_p + 2G + \Phi(D - N)\boldsymbol{n} : \boldsymbol{Z} - NKD} \tag{40}$$

In the case of isotropy ($\boldsymbol{Z} = 0$), Eq. (40) is reduced to the following familiar form [11]:

$$\Lambda = \frac{2G\boldsymbol{n} : \dot{\boldsymbol{e}} - NK\dot{\varepsilon}_v}{K_p + 2G - NKD} \tag{41}$$

Now, the stress rate tensor can be expressed by:

$$\dot{\boldsymbol{\sigma}} = 2G\dot{\boldsymbol{e}} + K\dot{\varepsilon}_v \boldsymbol{I} + \Phi[\boldsymbol{Z}\dot{\varepsilon}_v + (\boldsymbol{Z}:\dot{\boldsymbol{e}})\boldsymbol{I}]$$
$$- \langle \Lambda \rangle [2G\boldsymbol{n} + KD\boldsymbol{I} + \Phi D\boldsymbol{Z} + (\boldsymbol{Z}:\boldsymbol{n})\boldsymbol{I}] \qquad (42)$$

## 5. The Model Simulations

The modified model of this study introduces $\Phi$ as the sole new parameter to the basic critical state compatible bounding surface plasticity platform proposed by Dafalias and Manzari [18]. The calibration method of the basic model parameters is not described here and can be found elsewhere [11, 15, 18, 25]. For the new parameter, one can simply determine $\Phi$ through Eqs. (21) or (23) once $Z_{max}$ and $\beta_{TX}$ (or $\beta_{SS}$) are determined. In the absence of detailed data on slope of unloading curves, $\Phi$ may be estimated by Eq. (22).

In the following sub-sections, the modified model predictions are compared with the experimental data of six independent research groups on the mechanical behavior of Toyoura sand.

## 5.1. Simulation of Undrained Triaxial Loading-Unloading Tests

Verdugo and Ishihara [3] studied the behavior of Toyoura sand samples prepared by wet tamping method. In their testing program, isotropically consolidated samples were subjected to undrained triaxial loading-unloading shear. The 25% axial strain was selected as the utmost of the loading phase. When this strain limit was attained, samples were unloaded to zero shear stress under constant volume conditions in unloading phase. The results of four tests on medium-loose samples of the same density ($e = 0.833$, $Dr = 38\%$) starting at different values of mean principal effective stress ($p_{in} = 100$, 1000, 2000, and 3000 kPa) are presented in Figure (4). For three dense ($Dr = 56-66\%$) samples subjected to the loading-unloading pattern, the measured behaviors are presented in Figure (5). Using the model parameters given in Table (1), the mechanical behavior of seven tests described above are simu-
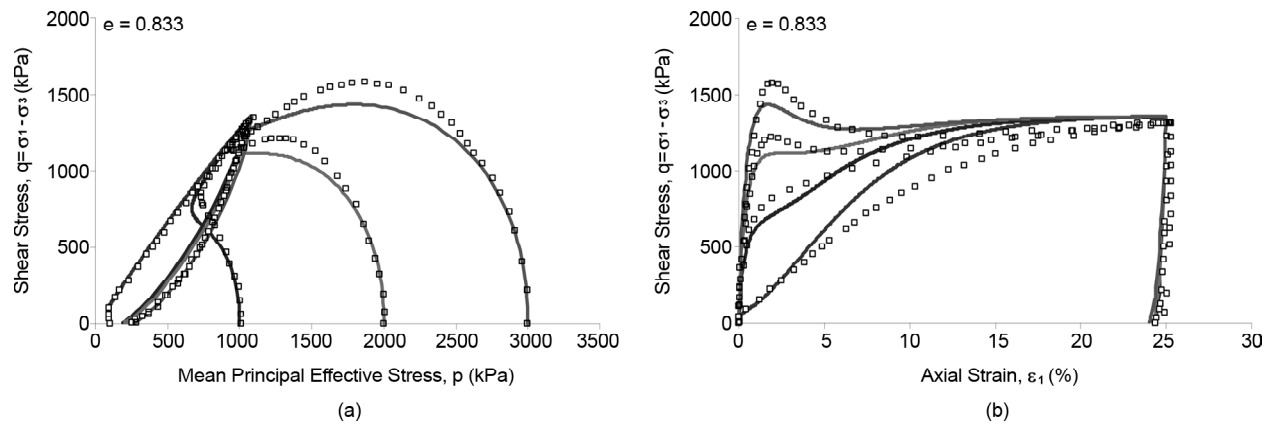


**Figure 4.** The modified model predictions versus experimental data of four undrained triaxial loading-unloading tests on medium-loose (Dr=38%, e=0.833) samples of Toyoura sand (data from [3]).
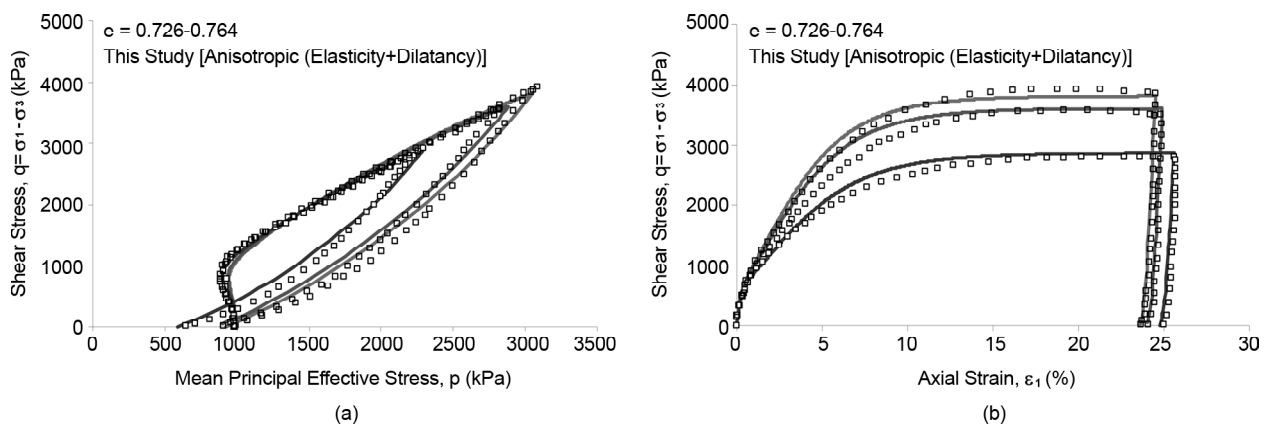


**Figure 5.** The modified model predictions versus experimental data of three undrained triaxial loading-unloading tests on dense (Dr ≈ 56-66%, e=0.726-764) samples of Toyoura sand (data from [3]).

**Table 1.** The model parameters used in simulations.

| | $G_0$ | $v$ | $m$ | $M$ | $c$ | $e_\Gamma$ | $\lambda$ | $\xi$ | $H(e)$ | $n_b$ | $n_d$ | $A$ | $Z_{max}$ | $c_z$ | $\|\beta_{TX}\|_{max}$ |
|---|---|---|---|---|---|---|---|---|---|---|---|---|---|---|---|
| Figures (4) to (8) | 125 | 0.05 | 0.01 | 1.25 | 0.75 | 0.934 | 0.019 | 0.70 | 2.46 (1.0 - 1.015e) | 1.1 | 3.50 | 0.70 | 2.0 | 1200 | 3.0 |
| Figures (9) to (14) | 125 | 0.05 | 0.01 | 1.25 | 0.75 | 0.976 | 0.026 | 0.70 | 430 $exp$(-9.0e) | 1.0 | 1.26 | 0.60 | 2.0 | 1200 | 3.0 |

lated and depicted together with the experimental data in Figures (4) and (5). For both loading and unloading phases, a reasonable correspondence between the experimental data and predictions exists.

### 5.2. Studies on the Influence of the Anisotropic Elements of the Model

By divesting the model from the elements introduced to take into account the effects of induced anisotropy, a number of stepwise studies on the influence of each element on the predictive capacity of the model are presented in Figure (6). To this end, predictions by the model of Manzari and Dafalias [11], which ignores the effect of induced anisotropy (the model employs isotropic elasticity defined through Eq. (3), and dilatancy function defined by $D=Ad:\boldsymbol{n}$); the model of Manzari and Dafalias [11] with the anisotropic elasticity of this study together with dilatancy function defined by $D=Ad:\boldsymbol{n}$ [instead of Eq. (37)]; and the model of Dafalias and Manzari [18], which only considers the influence of anisotropy on dilatancy through Eq. (37) are compared.

It must be noted that the model of [11] is the basic platform in all approaches. In part (a) of Figure (6), predictions by the model of Manzari and Dafalias [11] are compared with data. In all cases, the simulated mean principal effective stress is larger than the corresponding measured data. Moreover, a remarkable deviation from data can be observed in the slopes of stress paths immediately after the unloading points. These observations corroborate the model inability in the accurate simulation of the pore pressure build-up in reverse loading. Simulations by the model of Manzari and Dafalias [11] improved by the anisotropic elasticity theory of this study are presented in Figure (6b). A sharp shift is observed in unloading point of each stress path that fits well with the experimental data. As a result, a tangible improvement is achieved in all predictions compared to those obtained from
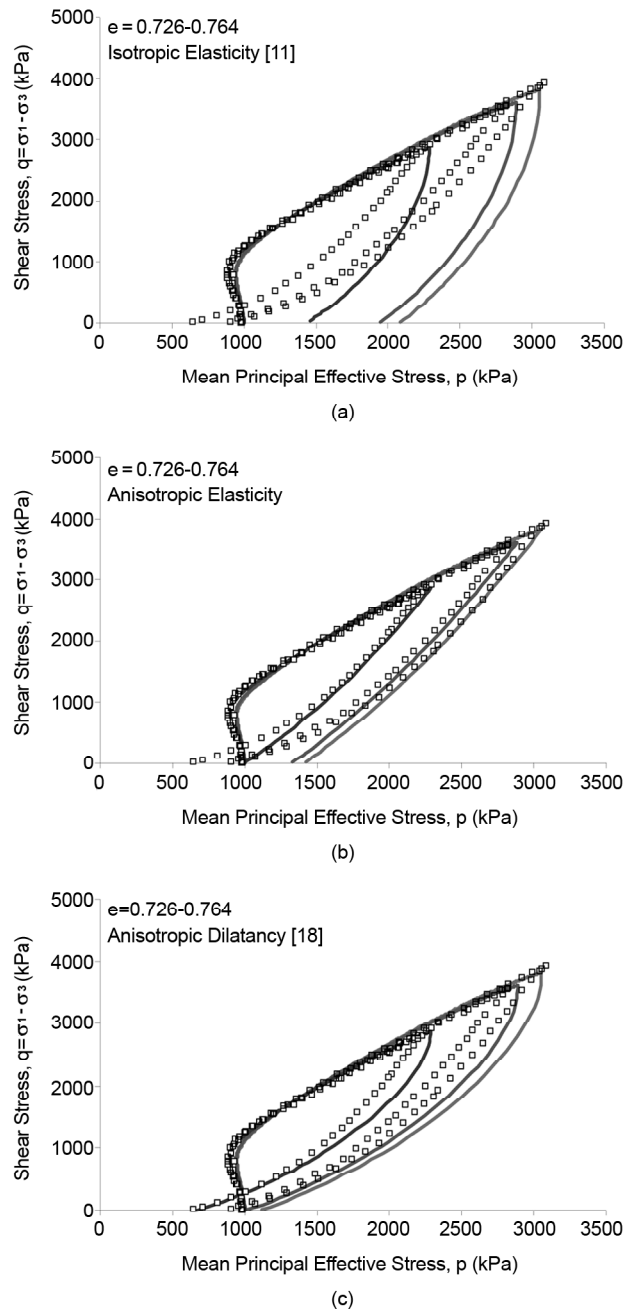


(a)



(b)



(c)

**Figure 6.** Experimental data of three undrained triaxial loading-unloading tests on dense (Dr $\approx$ 56-66%, e=0.726-764) samples of Toyoura sand versus the corresponding predictions obtained from: (a) the model of Manzari and Dafalias [11] which ignores the influence of induced anisotropy; (b) the model of Manzari and Dafalias [11] modified by the anisotropic elasticity of this study; (c) the model of Dafalias and Manzari [18] with anisotropic dilatancy and isotropic elasticity.

the basic model of Manzari and Dafalias [11]. Finally, predictions by the improved model of Dafalias and Manzari [18] by means of anisotropic dilatancy theory are depicted versus data in Figure (6c). One can find that considering the influence of induced anisotropy by relating dilatancy to a proper fabric-dilatancy tensor can lead to a remarkable improvement of predictions. Further comparison of predictions presented in parts "b" and "c" indicates that none of them is strictly successful in simulation of the sand response.

Referring to the part "b", the anisotropic elasticity fits data immediately after unloading when the mechanical behavior is mainly elastic. A different manner can be found in part "c". Due to the presence of isotropic elasticity, the model predictions lag behind data immediately after unloading. The gradual transition of behavior from elastic to elasto-plastic and the presence of anisotropic dilatancy function lead to the recovery of the model predictions in the medium to large stages of shear reversal. This brings us to the conclusion that the combined application of anisotropic elasticity and anisotropic dilatancy results in the best performance of the model over wide ranges of shear stress after reversal. Comparing part "a" of Figure (5) with simulations in Figure (6) confirms this idea. The measured stress path of the sample with $e = 0.726$ adjacent the unloading point is considered in Figure (7). The stress paths predicted by three approaches are identical prior to unloading, see path *AB* in Figure (7). As discussed before, isotropic elasticity theory predicts a vertical tangent to the stress path immediately after unloading in constant volume shear. This issue leads to a significant diversity observed between the prediction obtained from the model of Manzari and Dafalias [11] and the test result after the unloading point "B". However, the modification of dilatancy function by fabric-dilatancy tensor leads to refinement of the prediction of constitutive models in a butterfly loop, see Figure (6c), but this remedy is not functional immediately after unloading where the mechanical behavior is essentially elastic. Hence, the model of Dafalias and Manzari [18] is also unable to simulate the correct slope of stress path immediately after unloading.

The sensitivity of the model predictions with variation of $\beta_{max}$ (the only newly introduced model parameter) is studied in Figure (8). Investigation of
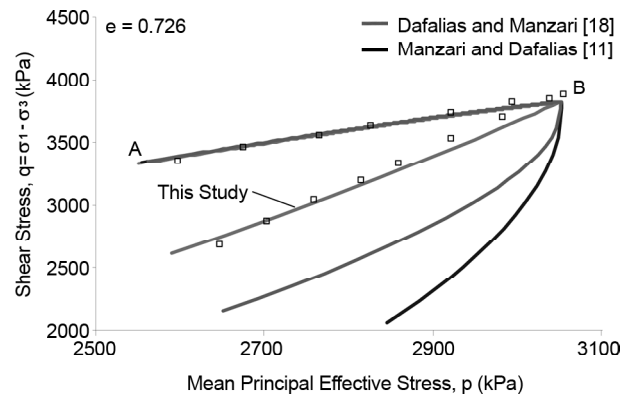


**Figure 7.** Comparison of predictions obtained from the modified model of this study with anisotropic elasticity, the model of Dafalias and Manzari [18] with modified dilatancy function with fabric-dilatancy tensor, and the original framework of Manzari and Dafalias [11] in simulation of undrained triaxial loading-unloading stress path (data from [3]).
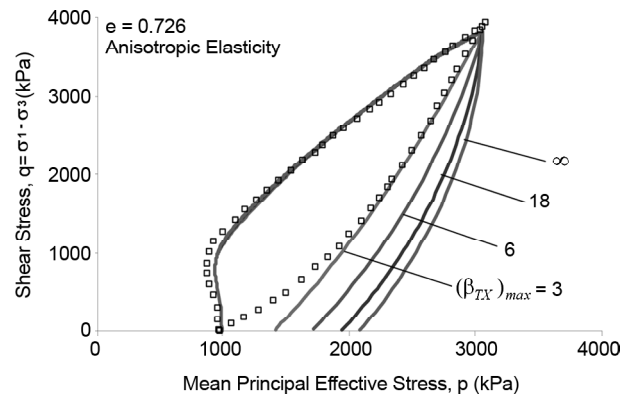


**Figure 8.** A sensitivity study on the influence of $(\beta_{TX})_{max}$ on the model predictions.

the behavior of various sands indicates that the typical value of $|\beta_{max}| \approx 3.0$ is a reasonable assumption. The slope of the unloading path deviates from the measured data with the increase of $\beta_{max}$. Ultimately by setting $\beta_{max} = \infty$, the model prediction transforms to that of Manzari and Dafalias [11] with isotropic elasticity.

### 5.3. Simulation of Liquefaction in Cyclic Triaxial Tests

Numerous researchers have studied monotonic and cyclic behavior of Toyoura sand samples prepared by dry deposition method [e.g., 4-8]. However, reliable published works in which the monotonic and cyclic behaviors are simultaneously studied are scarce. To overcome this difficulty, by using experimental data of three independent

researches on the monotonic response of dry deposited Toyoura sand samples, the model parameters associated with this fabric are determined. Using these parameters which are given in Table (1), behavior of ten samples under monotonic constant volume triaxial loading are simulated and illustrated with corresponding data in Figures (9) to (11). Once

again, a reasonable agreement is found between the model predictions and the experiments which are separately conducted. This issue becomes more interesting when it is indicated that the values of void ratio and mean principal effective stress cover wide ranges of variation in tests. The existing consistency justifies the propriety of the proposed parameters
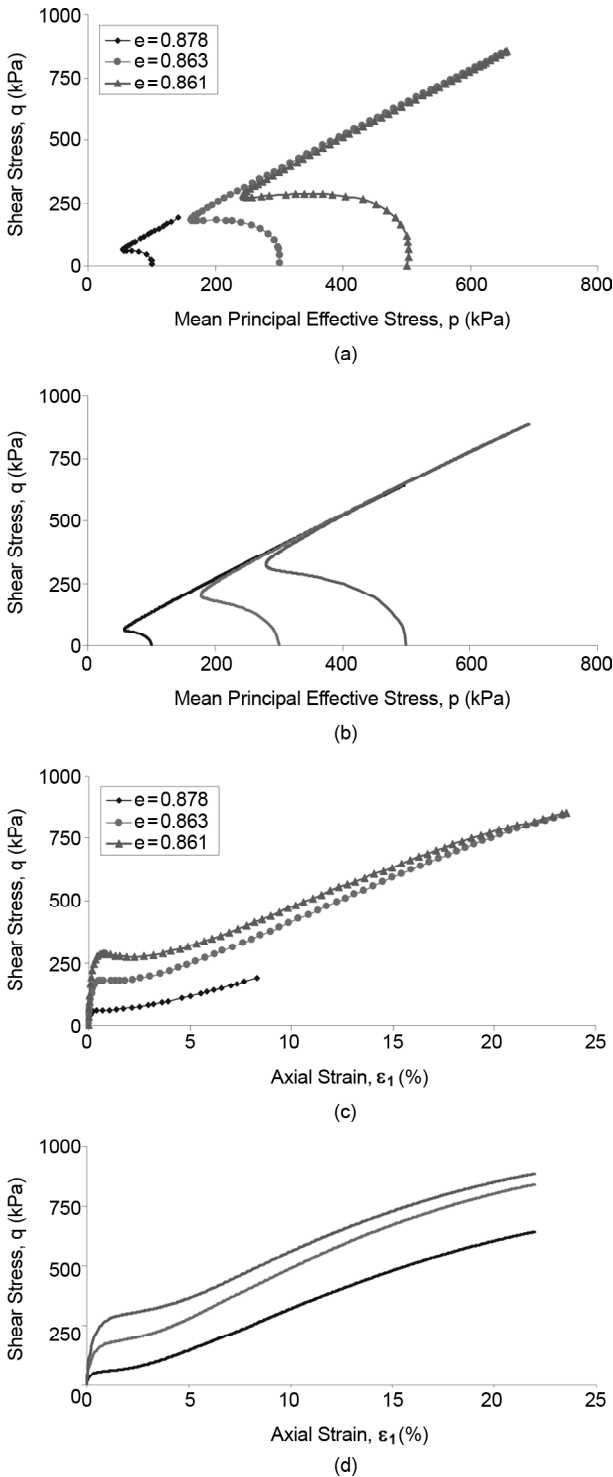


**Figure 9.** The modified model predictions versus experimental data of three undrained triaxial tests on medium-loose samples of Toyoura sand (data from [4]).
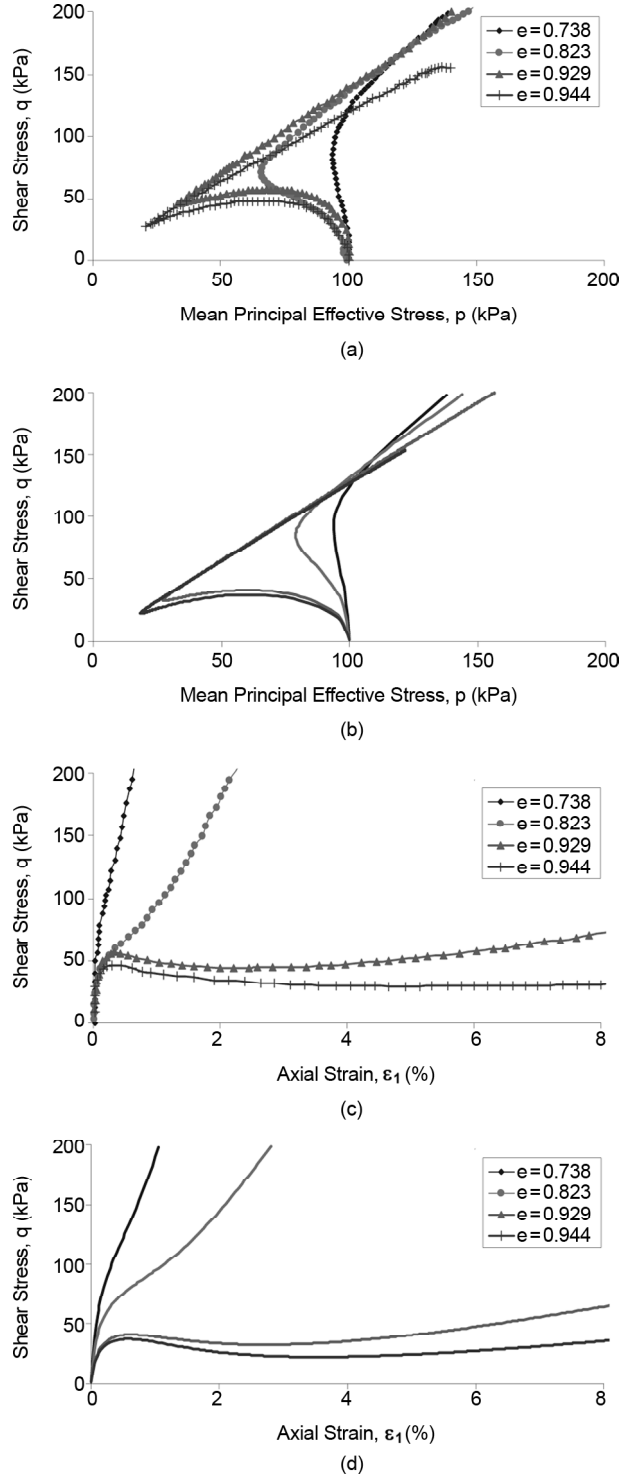
**Figure 10.** The modified model predictions versus experimental data of four undrained triaxial tests on dense to very loose samples of Toyoura sand (data from [19]).

for simulation of the mechanical behavior of dry deposited samples of Toyoura sand. Using these parameters, three cyclic tests reported by two other research teams are simulated and comparisons are shown in Figures (12) to (14). In this regard, results of a cyclic test on a dense sample of Toyoura sand started at $p$=100$kPa$ is taken from Yoshimine and
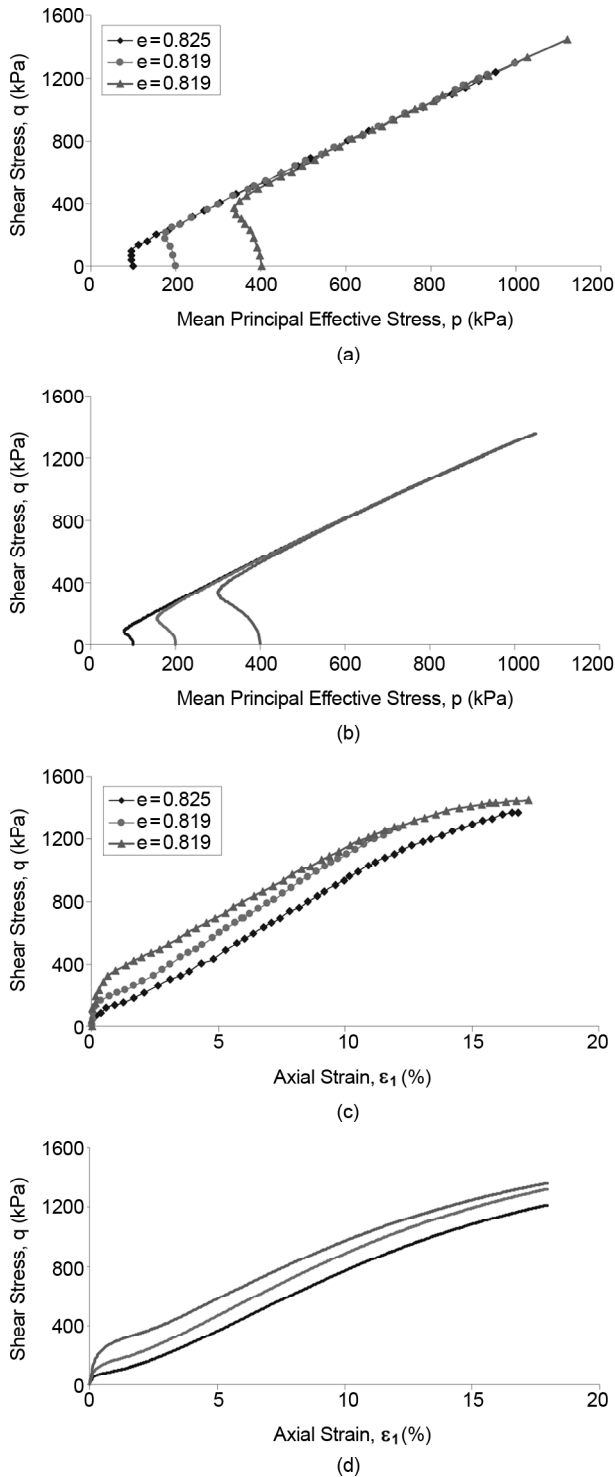


Figure 11. The modified model predictions versus experimental data of three undrained triaxial tests on medium-loose samples of Toyoura sand (data from [7]).
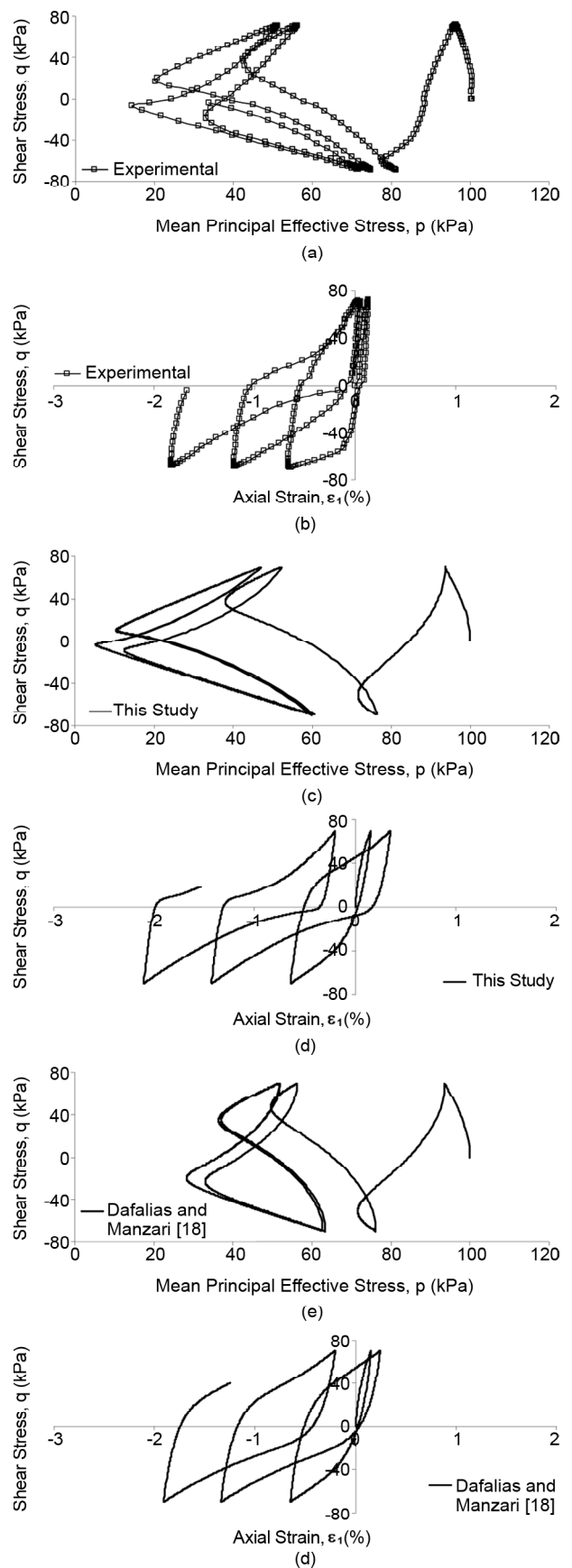


**Figure 12.** Comparisons between the data of a triaxial test and simulations: (a) and (b) test data [6]; (c) and (d) simulations obtained from the modified model of this study with anisotropic elasticity for e=0.74; (e) and (f) simulations for e = 0.74 by the model of Manzari and Dafalias [11].
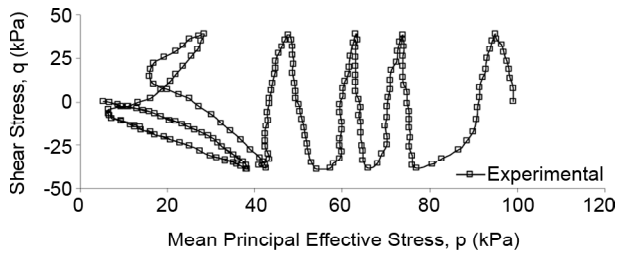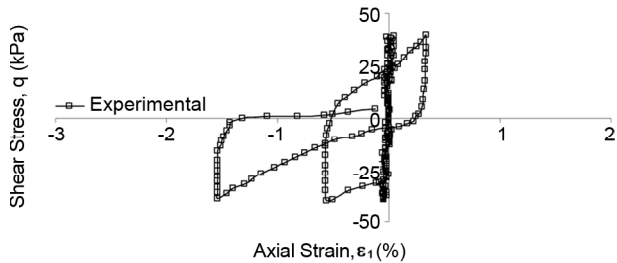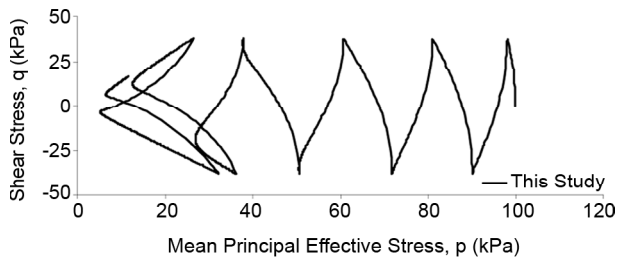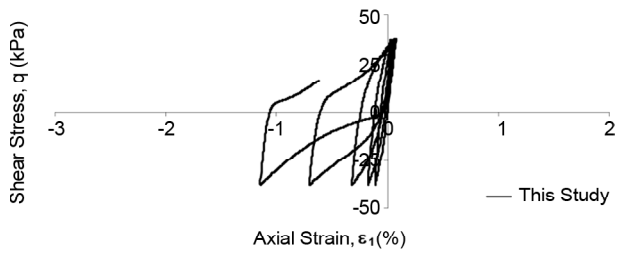
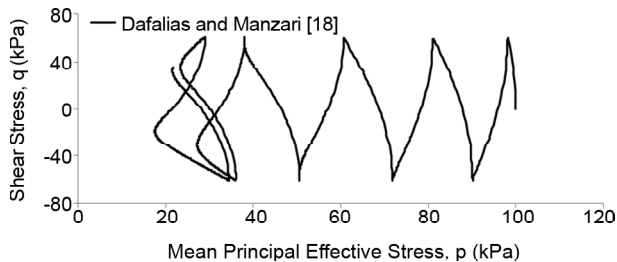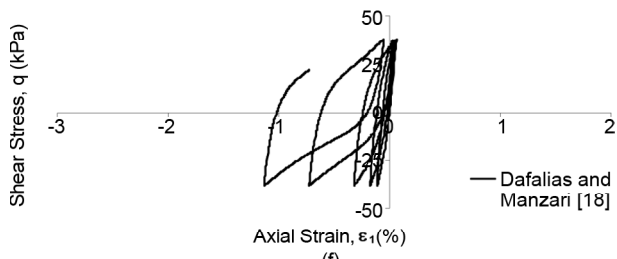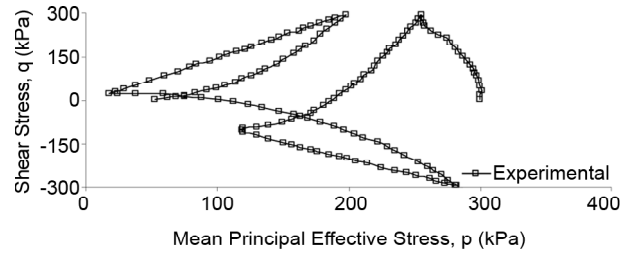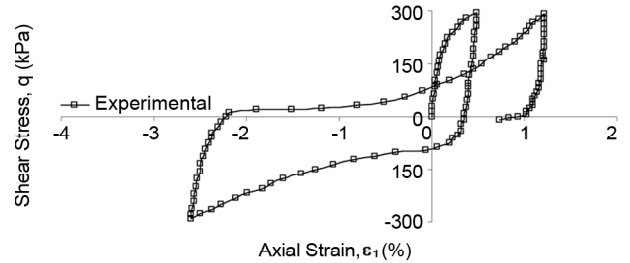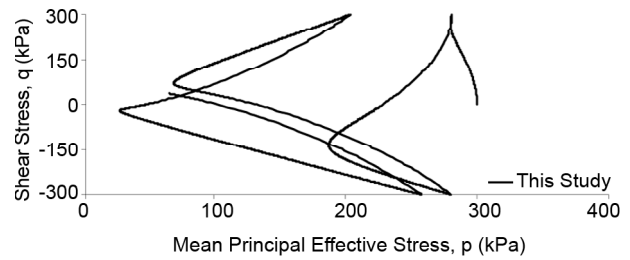**Figure 13.** Comparisons between the data of a triaxial test and simulations: (a) and (b) test data [8]; (c) and (d) simulations obtained from the modified model of this study with anisotropic elasticity for e=0.73; (e) and (f) simulations for e=0.73 by the model of Manzari and Dafalias [11].

**Figure 14.** Comparisons between the data of a triaxial test and simulations: (a) and (b) test data [8]; (c) and (d) simulations obtained from the modified model of this study with anisotropic elasticity for e=0.72; (e) and (f) simulations for e=0.72 by the model of Manzari and Dafalias [11].
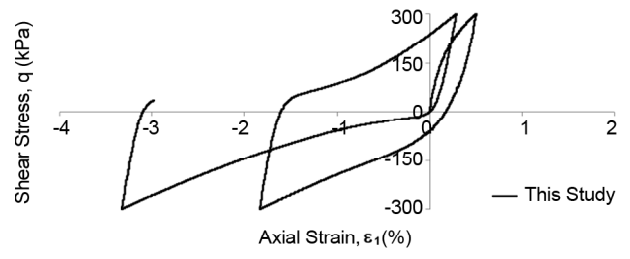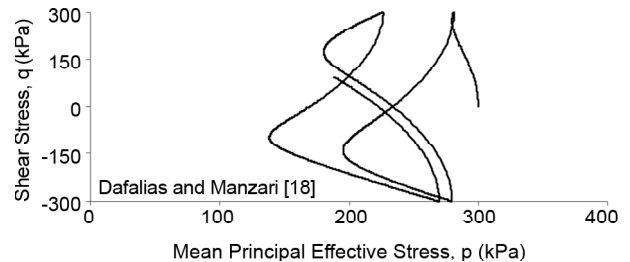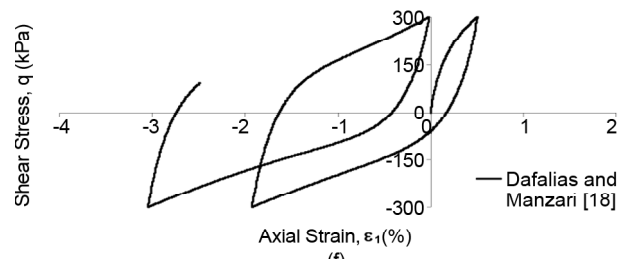
Hosono [6]. During the test, magnitude of cyclic shear stress is bounded between +70 and -70$kPa$. At the second reversal, the sample state enters the butterfly loop which is the first sign of coming liquefaction, and 85$kPa$ pore water pressure is accumulated in the third cycle, see parts "a" and "b" of Figure (12). The modified model predictions are presented in parts "c" and "d" of Figure (12). For the aim of comparison, simulation obtained from the model of Manzari and Dafalias [11] are presented in parts "e" and "f" of Figure (12). Using the same preparation method, more recently, Yamada et al [8] studied the cyclic behavior of dense samples of Toyoura sand. Two series of evaluations are organized here using those tests without previous shear history. The first test performed on a sample isotropically consolidated at $p=100kPa$ and the shear stress oscillating in range of $q=\pm39kPa$. The stress path and shear stress versus axial strain of this test are illustrated in parts "a" and "b" of Figure (13). Unlike the previous test and due to the lower amplitude of the applied shear stress, the sample enters the butterfly loop in the fifth cycle. In the same cycle, nearly 92$kPa$ pore water pressure is accumulated. The last set of comparisons is presented in Figure (14) using data of another test by Yamada et al [8] that is started at $p=300kPa$ with the maximum shear amplitude in the range $q=\pm300kPa$. This sample steps in the butterfly loop in the first cycle, and a maximum of 285$kPa$ pore water pressure built up is recorded in the second cycle of shearing. Predictions calculated by the modified model of this study, and by the basic framework of Manzari and Dafalias [11] are presented in Figures (13) and (14). Like the previous simulations, it is observed that inclusion of anisotropic elasticity results in a concrete improvement of simulations in the butterfly loop. All simulations presented in Figures (9) to (14) are obtained from a unique set of model parameters; however, refined predictions may be achieved for each set of simulations by imposing small variation on the parameters.

## 6. Conclusions

Comparing to other engineering materials, the mechanical behavior of granular soils is considered complex because it may be highly non-linear, highly state dependent, and also highly anisotropic. In the constitutive modeling of the non-linearity and state

dependency of sands, a remarkable success has been achieved in the last decades. Regarding the anisotropy, various aspects of the anisotropic nature of granular soils are considered in the constitutive models proposed in the recent years. However, in order to avoid complexity, the possibility of the anisotropic elasticity is usually ignored in formulation of these constitutive models. Herein, a simplified anisotropic elasticity was proposed by incorporation of an evolving fabric-dilatancy tensor in the elasticity tensor. Attempt has been made to keep the formulation as simple as possible and compatible with other fabric dependent ingredients of the existing constitutive models. It was shown that only one new parameter is required for the suggested elasticity theory which can easily be calibrated using the results of conventional constant volume tests. The introduced anisotropic elasticity was implemented in a multiaxial bounding surface plasticity model. It was shown that considering the possibility of anisotropic elasticity leads to the improvement of predictions for liquefaction under cyclic shear loads.

## References

1. Ishihara, K., Haeri, S.M., Moinfar, A.A., Towhata, I., and Tsujino, S. (1992). "Geotechnical Aspects of the June 20, 1990 Manjil Earthquake in Iran", *Soils and Foundations*, **32**(3), 61-78.

2. Been, K. and Jefferies, M.G. (1985). "A State Parameter for Sands", *Géotechnique*, **35**(2), 99-112.

3. Verdugo, R. and Ishihara, K. (1996). "Steady State of Sandy Soils", *Soils and Foundations*, **36**(2), 81-91.

4. Yoshimine, M., Ishihara, K., and Vargas, W. (1998). "Effect of Principal Stress Direction and Intermediate Principal Stress on Undrained Shear behavior of Sand", *Soils and Foundations*, **38**(3). 179-188.

5. Koseki, J., Kawakami, S., Nagayama, H., and Sato, T. (2000). "Change of Small Strain Quasi-Elastic Deformation Properties During Undrained Cyclic Torsional Shear and Triaxial Tests of Toyoura Sand", *Soils and Foundations*, **40**(3), 101-110.

6. Yoshimine, M., and Hosono, Y. (2000). Effects of

Anisotropy of Sand on Results of Undrained Triaxial Tests", Memoirs of Graduate School of Engineering of Tokyo Metropolitan University, No. 50, 158-169.

7. Yang, Z.X., Li, X.S., and Yang, J. (2008). "Quantifying and Modeling Fabric Anisotropy of Granular Soils", *Géotechnique*, **58**(4), 237-248.

8. Yamada, S., Takamori, T., and Sato, K. (2010). "Effects of Reliquefaction Resistance Produced by Changes in Anisotropy during Liquefaction", *Soils and Foundations*, **50**(1), 9-25.

9. Prevost, J.H. (1985). "A Simple Plasticity Model for Frictional Cohesionless Soils", *Soil Dynamics and Earthquake Engineering*, **4**(1), 9-17.

10. Pastor, M., Zienkiewicz, O.C., and Chan, A.H.C. (1990). "Generalized Plasticity and Modeling of Soil behavior", *International Journal for Numerical Methods in Geomechanics*, **14**, 151-190.

11. Manzari, M.T., and Dafalias, Y.F. (1997). "A Critical State Two Surface Plasticity Model for Sands", *Géotechnique*, **44**(2), 255-272.

12. Wan, R.G., and Guo, P.J. (1998). "A Simple Constitutive Model for Granular Soils: Modified Stress-Dilatancy Approach", *Computers and Geotechnics*, **22**(2), 109-133.

13. Pestana, J.M. and Whittle, A.J. (1999). "Formulation of a Unified Constitutive Model for Clays and Sands", *International Journal for Numerical and Analytical Methods in Geomechanics*, **23**, 1215-1243.

14. Wan, R.G. and Guo, P.J. (2001). "Effect of Microstructure on Undrained behavior of Sand", *Canadian Geotechnical Journal*, **38**, 16-28.

15. Papadimitriou, A.G. and Bouckovalas, G.D. (2002). "Plasticity Model for Sand under Small and Large Cyclic Strain: A Multiaxial Formulation", *Soil Dynamics and Earthquake Engineering*, **22**(3), 191-204.

16. Wang, Z.L., Dafalias, Y.F., Li, X.S., and Makdisi, F.I. (2002). "State Pressure Index for Modeling Sand behavior", *ASCE Journal of Geotechnical and Geoenvironmental Engineering*, **128**(6), 511-519.

17. Byrne, P.M., Park, S.S., Beaty, M., Sharp, M.K., Gonzalez, L., and Abdoun, T. (2004). "Numerical Modeling of Liquefaction and Comparison with Centrifuge Tests", *Canadian Geotechnical Journal*, **41**(2), 193-211.

18. Dafalias, Y.F. and Manzari, M.T. (2004). "Simple Plasticity Model Accounting for Fabric Change Effects", *ASCE Journal of Engineering Mechanics*, **130**(6), 622-634.

19. Papadimitriou, A.G., Dafalias, Y.F., and Yoshimine, M. (2005). "Plasticity Modeling of the Effect of Sample Preparation Method on Sand Response", *Soils and Foundations*, **45**(2), 109-123.

20. Bolton, M.D. (1986). "The Strength and Dilatancy of Sands", *Géotechnique*, **36**(1), 65-78.

21. Cubrinovski, M. and Ishihara, K. (1998). "State Concept and Modified Elastoplasticity for Sand Modeling", *Soils and Foundations*, **38**(4), 213-225.

22. Lashkari, A. (2009). "On the Modeling of the State Dependency of Granular Soils", *Computers and Geotechnics*, **36**, 1237-1245.

23. Muir Wood, D., Belkheir, K., and Liu, D.F. (1994). "Strain Softening and State Parameter for Sand Modeling", *Géotechnique*, **44**(2), 335-339.

24. Latifi, M. (1998). "A Multi-Yield Surface Model in Reference State Soil Mechanics for Cohesionless Soils and Liquefaction Problems", Ph.D Thesis, University of Alberta, Canada.

25. Papadimitriou, A.G., Bouckovalas, G.D., and Dafalias, Y.F. (2001). "Plasticity Model for Sand under Small and Large Cyclic Strains", *ASCE, Journal of Geotechnical and Geoenvironmental Engineering*, **127**(11), 973-983.

26. Lashkari, A. and Latifi, M. (2007). "A Simple Plasticity Model for Prediction of Non-Coaxial Flow of Sand", *Mechanics Research Communications*, **34**, 191-200.

27. Oda, M. and Konishi, J. (1974). "Microscopic Deformation Mechanism of Granular Material in Simple Shear", *Soils and Foundations*, **14**(4), 25-38.

28. Chen, Y-C. and Ishibashi, I. (1990). "Dynamic Shear Modulus and Evolution of Fabric of Granu

lar Materials", *Soils and Foundations,* **30**(3), 1-10.

29. Thornton, C. (2000). "Numerical Simulation of Deviatoric Shear Deformation of Granular Media", *Géotechnique,* **50**(1), 43-53.

30. Seyedi Hosseininia, E. and Mirghasemi, A.A. (2007). "Effect of Particle Breakage on the Behavior of Simulated Angular Particle Assemblies", *China Particuology,* **5**(5), 328-336.

31. Yunus, Y., Vincens, E., and Cambou, B. (2009). "Numerical Local Analysis of Relevant Internal Variables for Constitutive Modeling of Granular Materials", *International Journal for Numerical and Analytical Methods in Geomechanics,* **34**(11), 1101-1123.

32. Graham, J. and Houlsby, G.T. (1983). "Anisotropic Elasticity of Natural Clay", *Géotechnique,* **33**(2), 165-180.

33. De Gennaro, V., Canou, J., Dupla, J.C., and Benahmed, N. (2004). "Influence of Loading Path on the Undrained behavior of a Medium Loose Sand", *Canadian Geotechnical Journal,* **41**, 166-180.

34. Muir Wood, D. (2006). "Soil: Discontinuum-Continuum", Lecture Papers, the International Symposium on Geomechanics and Geotechnics of Particulate Media (IS-Yamaguchi), Ube, Japan.

35. Tobita, Y. (1989). "Fabric Tensors in Constitutive Equations for Granular Materials", *Soils and Foundations,* **29**(4), 99-104.

36. Truesdell, C. and Noll, W. (1965). "The Non-Linear Field Theories of Mechanics", In: S. Flugge, Ed., Handbuch der Physik III/3.

37. Cowin, S.C. (1985). "The Relationship between the Elasticity Tensor and the Fabric Tensor", *Mechanics of Materials,* **4**, 137-147.

38. Oda, M. (1999). "Fabric Tensor and Its Geometrical Meaning", *Introduction to Mechanics of Granular Materials,* M. Oda and K. Iwashita Eds., A.A. Balkema, Rotterdam, The Netherland, 27-35.

39. Satake, M. (1983). "Fundamental Quantities in the Graph Approach to Granular Materials", Mechanics of Granular Materials: New Models and Constitutive Relations (Jenkins and Satake, Eds.), Elsevier Science Pub.

40. Nemat-Nasser, S. and Mehrabadi, M.M. (1983). "Stress and Fabric in Granular Mass", Mechanics of Granular Materials: New Models and Constitutive Relations (Jenkins and Satake, Eds.), Elsevier Science Pub.

41. Oda, M., Nemat-Nasser, S., and Konishi, J. (1985). "Stress Induced Anisotropy in Granular Masses", *Soils and Foundations,* **25**(3), 85-97.

42. Hardin, B.O. and Richart, F.E. (1963). "Elastic Wave Velocities in Granular Soils", *ASCE, Journal of Soil Mechanics and Foundations,* **89**(SM1), 33-65.